RSC Advances

ROYAL SOCIETY OF CHEMISTRY

www.rsc.org/advances

Cite this: DOI: 10.1039/c0xx00000x

www.rsc.org/xxxxxx

ARTICLE TYPE

A molecularly imprinted electrochemical enzymeless sensor based on functionalized gold nanoparticles decorated carbon nanotubes for methyl-parathion detection

Bowan Wu[a,b], Lijie Hou[a], Miao Du[a], Tiantian Zhang[a], Zhihua Wang[b], Zhonghua Xue[b], Xiaoquan Lu[b]*

Received (in XXX, XXX) Xth XXXXXXXXX 20XX, Accepted Xth XXXXXXXXX 20XX
DOI: 10.1039/b000000x

Functionalized gold nanoparticles (FuAuNP) have a bright future because of its specific functional groups. *p*-Aminothiophenol (*p*-ATP) possesses double functional groups which can be used to form S-Au bond and oligoaniline. Based on molecular imprinting technology and electrochemical technology, a novel enzymeless Methy-parathion (MP) sensor is constructed with nanocomposites. The template molecule (MP) is embedded in imprinting sites by *p*-ATP molecular self-assembly and FuAuNP electro-polymerization. The imprinting effective sites and the conductive performance are improved by gold nanoparticles decorated carbon nanotubes nanocomposites (AuNP-MCNT). The linear relationships between peak current and MP concentration are obtained in the range from 0.1 to 1.1 ng mL^{-1} and 1.1 to 11 ng mL^{-1} (respectively). The detection limit can be achieved as low as 0.08 ng mL^{-1} (3σ) with relative standard deviation 3.8% (n = 5). This sensor was also applied in the detection of MP in appler and vegetables with average recoveries between 95.2% and 105.7% (RSD < 5%). The results mentioned above show that the novel electrochemical sensor is an ideal device for the real-time determination of MP in real samples.

Introduction

With the development of intensive agricultural practices, pesticides (herbicides, fungicides, insecticides) are widely used throughout the world, and millions of tons of pesticides are used each year in agriculture, medicine, industry and related activities[1]. Methyl-parathion (MP) as a kind of organophosphorus pesticide is widely used in agriculture due to their high toxicity to insects and limited persistence in the environments [2-4]. Nevertheless, low levels of MP pesticides in agricultural products and the natural environment is extremely harmful to human health and zoology. Nowadays, these are many classical methods for the detection of MP [5-11], they are high efficiency and allow discrimination among different types of organophosphorus compounds, but they are expensive, time-consuming, and sometimes require highly qualified technicians and not apt for real-time detection. Furthermore, enzyme/antibody-based immunoassay has also been developed for the detection of organophosphate [12-19]. However，the antibodies or enzymes can be easily destroyed in the harsh and high temperature environments due to its poor chem-physical stability. Accordingly, it is still a great challenge to develop a rapid, inexpensive, reliable and sensitive method for the detection of MP in environments[20, 21].

Because of its high selective recognition and a wide choice of templates and functional monomers, molecular imprinting technique (MIT) has attracted increased attention [22-27]. Owing to its unique advantages over natural biological receptors in terms of physical and chemical stability, ease of preparation, low cost, and applicability in harsh environmental conditions[28-30], molecularly imprinted polymers (MIP) have been widely explored for mimicing natural receptors[31-33]. However, a variety of traditional imprinted materials suffer from some drawbacks including small binding capacity, slow mass transfer and irregular material shape[34, 35]. As we all know, the quantity of effective recognition sites and conductivity determine the sensitivity of the imprinted sensor. Binding sites increased with the thickness of imprinted membrane, but thick imprinted membranes can lead to slow diffusion of the analytes to the recognition sites and inefficient communication between the imprinted sites and the transducers[36]. To further increase the amount of effective binding sites on the sensor surface, the simplest solution is to modify present electrode through the assembly of nanoparticles, by which the resulting electrode can offer high conductivity, large specific surface area, and good biocompatibility. In recent years, scientists have made considerable efforts to overcome these problems by adapting the nanofabrication technique for example in the preparation of mesoporous silica particles and polyaniline

[a] *LONGDONG UNIVERSITY-FLUOBON Surfactant Engineering Technology Center, College of Chemistry & Chemical Engineering, Cooperative Innovation Center of Industrial Surfactant, Longdong University, 45 Lanzhou Road, Qingyang China. Fax: +86-931-7971323; Tel: +86-15701709818; E-mail: qywbowan@gmail.com*
[b] *Key Laboratory of Bioelectrochemistry & Environmental Analysis of Gansu Province, College of Chemistry & Chemical Engineering, Northwest Normal University, 967 Anning East Road, Lanzhou, China. Fax: +86-931-7971323; Tel: +86-931-7971276 E-mail: luxq@nwnu.edu.cn*

nanofibers [37, 38]. This technique is based on the small dimension with extremely high surface-to-volume ratio of nano-imprinting materials, which enable the imprinting technique to create more effective recognition sites than those obtained by traditional approaches which only use porogens [38, 39].

Furthermore, carbon nanotubes (CNT)[40] are ideal materials for construction of electrochemical sensors due to their exceptional mechanical properties, unique electrical properties, high surface area, high aspect ratio, and enhanced catalytic properties. Accordingly, researchers have continue to develop novel uses for these nanomaterials in electrochemical sensors at a rapid pace [41-44]. Gold nanoparticles (AuNP) are being used increasingly in many electrochemical applications since they have the ability to enhance the electrode conductivity and facilitate the electron transfer [45, 46]. More recently, integration of metallic nanoparticles with CNT has attracted much interest in the construction of electrochemical sensors because of the low resistance ohmic contacts of these composites [19, 47, 48]. In addition, these nano-hybrid materials often exhibit interesting properties that are not available to the respective components alone. Therefore, nano-hybrid materials can offer new opportunities for the development of new sensors and biosensors with high analytical performance [49-53]. Electrochemical techniques have many advantages in the sensors field including low cost, simplicity, easy miniaturization and automation, high stability, and so on. Molecularly imprinted electrochemical sensors (MIECS) combine the advantage of both MIT and electrochemical sensors, and are widely used in the research of environmental monitoring[54], biological/chemical analysis[55], pharmaceutical analysis[56], residue detection of pesticides and overdose[57, 58], and so on.

In this paper, a novel sensor for determination MP based on MIP and electrochemical technology was constructed. Molecularly imprinted film was modified on the electrode surface, and MP was linked to the cavities constructed by binding sites of molecularly imprinted film. We hypothesized the combination of surface molecular self-assembly and hybrize nanomaterials with polymerization of the functionalized gold nanoparticles (FuAuNP) and template molecule (MP) on glass carbon electrode (GCE) will produce the total amount of effective imprinted sites and enhance its conductivity. The nanocomposites film has a high stability since AuNP/MCNT can succeed in being incorporated into the latticework of the formation of FuAuNP-ATP film. So we developed a new electrochemical sensors which is sensitive to detect MP.

Experimental

Materials and chemicals

Multi-walled carbon nanotubes (MCNT) with diameter of 20-40nm are obtained from Shenzhen Nanotech Port Co., Ltd. Hydrochloroauric acid ($HAuCl_4 \cdot 4H_2O$) is obtained from Shanghai Chemical Factory. Nafion solution (perfluorinated ion-exchange powder 5 wt% solution in a mixture of lower aliphatic alcohols and water, DE520) is obtained from DuPont Co. Methyl-parathion (MP) and *p*-aminothiophenol (*p*-ATP) is obtained from Aladdin Chemistry Co. Ltd. 2-mercaptoethane sulfonic acid is purchased from TCI (Shanghai, China) development Co., Ltd. All other reagents are at least analytical reagent grade. Phosphate buffer solution (PBS) is prepared by using disodium hydrogen phosphate (Na_2HPO_4) and sodium dihydrogen phosphate (NaH_2PO_4), and the buffer is adjusted to appropriate pH with sodium hydroxide (NaOH) and phosphoric acid (H_3PO_4). Stock solution of MP is prepared with ethanol and kept in refrigerator at about 4℃. Double distilled water is used in all aqueous solution preparation and washings. High-purity N_2 is used. All experiments are carried out at ambient temperature.

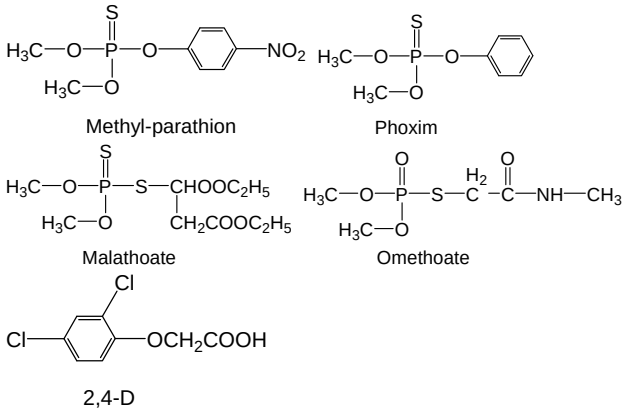

Scheme 1. Structural formulas of the pesticide compounds used in this study

Apparatus

Electrochemical measurements were carried out on a CHI832 electrochemical workstation (ChenHua Instruments Co., Shanghai, China) with a conventional three electrode system comprising platinum wire as auxiliary electrode, Ag/AgCl electrode as reference and the bare or modified glass carbon electrode (GCE) or MIP electrode as working electrode. Electrochemical impedance spectroscopy (EIS) experiments were performed on a VMP2 Multi-potentiostat (Princeton Applied Research, USA), which was controlled by EC-Lab (V9.24) software (Bio- Logic SA). UV-vis absorption spectra were taken by absorption mode with a UV-1102 UV-vis spectrophotometer (Shanghai, China). The surface morphologies and size distribution of the prepared electrodes were characterized by using a Field-emission Scanning Electron Microscope (FESEM; JEOL JSM-6701F, operating at 5 keV). High-resolution Transmission Electron Microscopy (HRTEM) was performed by using a FEI Tecnai TF20 TEM operated at 200 kV. For TEM measurement, the sample was suspended in double distilled water solution and was drop cast onto carbon-coated copper grid followed by solvent evaporation in air at room temperature. X-ray powder diffraction (XRD) data was obtained by an X' Pert PRO Multi-purpose Diffractometer (PANalytical, Netherlands) using Cu K_α radiation (k=0.15418nm). The pH measurements were performed with PB-10 pH meter (Sartorius, Germany).

Preparation of MP MIP Electrochemical Sensor

Prior to modification, the GCE was polished with 0.3 and 0.05μm alumina slurry and rinsed thoroughly with doubly distilled water between each polishing step. Then, it was washed successively with doubly distilled water and ethanol in an ultrasonic bath, and finally dried with high purity nitrogen steam at room temperature.

Preparation of Functionalized AuNP

Au nanoparticles functionalized with 2-mercaptoethane sulfonic

acid and *p*-ATP (FuAuNP) were prepared by mixing a 10 mL solution containing 197 mg of $HAuCl_4$ in ethanol and a 5 mL solution containing 42 mg of mercaptoethane sulfonate and 8mg of *p*-ATP in methanol. The two solutions were stirred in the presence of 2.5 mL of glacial acetic acid in an ice bath for 1h. Subsequently, 7.5 mL of aqueous solution of 1M sodium borohydride, $NaBH_4$, was added dropwise, resulting in a dark color solution associated with the presence of the AuNP. The solution was stirred for 1h additionally in an ice bath and then for 14h at room temperature. The particles were successively washed and centrifuged (twice in each solvent) with methanol, ethanol, and diethyl ether. The TEM image of the FuAuNP is shown in Fig. 1. The particle has a size less than 5 nm and distribute uniformly with spherical morphologies, which may be related to the preparation method used in this work. The FuAuNP shows good monodisperse distribution, without obvious aggregation in copper net of TEM, which suggests that the surface functionalization is effective to improve the dispensability of AuNP. The electron diffraction graph(See Fig. 1B) of FuAuNP is the typical diffraction pattern of metal particles, implying a polycrystalline characteristic.

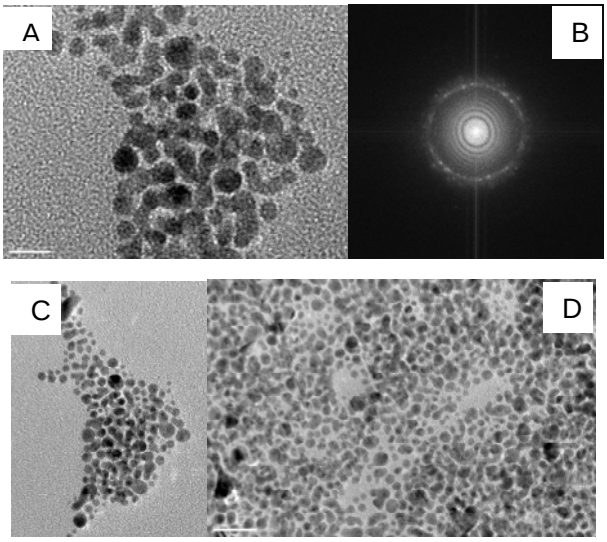

Fig.1. (A), (C) and (D): TEM images of FuAuNP in different resolution. (B): The electron diffraction graph of FuAuNP.

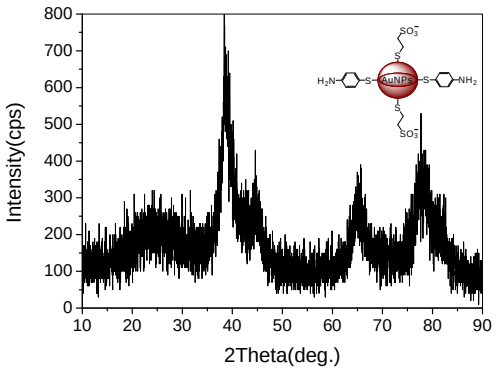

Fig. 2. XRD pattern of FuAuNP.

The XRD pattern of FuAuNP (See Fig. 2) shows five diffraction peaks appeared at 2θ of 38.6°, 44.4°, 64.9°, 77.5° and 82.2°, which can be ascribed to (1 1 1), (2 0 0), (2 2 0), (3 1 1) and (2 2 2) planes of Au face-centered cubic crystallographic structure. According to the Scherrer equation [59, 60], the average diameter of the FuAuNP was calculated to be 3.5 nm, which is consistent with previous reports [61-65].

Preparation of the molecularly imprinted electrochemical enzymeless sensor

The carboxylic acid-functionalized MCNT (MCNT-COOH) were synthesized according to the published method[66] and the MCNT modified GCE(MCNT/GCE) were obtained according to our previous research[67]. To electrodeposit AuNP on the surface of the MCNT/GCE, MCNT/GCE was immersed into 0.2 M Na_2SO_4 solution containing 1mM $HAuCl_4$. The modification of AuNP onto MCNT/GCE was conducted by CV scanning from -0.2 to 1.0 V with a scan rate of 50 mV s^{-1} for 6 cycles (Fig. 3A). The AuNP-MCNT hybrid modified GCE (AuNP-MCNT/GCE) was taken out and rinsed with doubly distilled water and finally blew dry with nitrogen. To obtain MP-ATP-AuNP-MCNT/GCE, the AuNP-MCNT/GCE was immersed in 0.1M phosphate buffer solution (PBS, pH 7.4) containing 1 mM *p*-ATP and 1 mM MP for 2h. Finally, the MP-ATP-AuNP-MCNT/GCE was immersed in PBS (pH 7.4) that contained 1 mg mL^{-1} of FuAuNP and 0.2 mg • mL^{-1} MP. The polymerization was performed by the application of 15 potential cycles between –0.35 and 0.5 V, with a potential scan rate of 50 mV s^{-1} [36, 68, 69] (Fig. 3B). After the electropolymerization, the composite membrane modified electrode (FuAuNP-ATP-MIP-AuNP-MCNT/GCE) was washed with the background electrolyte solution to exclude any residual monomer in the electrode. Then the imprinted electrode was rinsed with double distilled water and finally dried under nitrogen for further usage. Similarly, a non-MIP control electrode was prepared by following the same procedure but without MP template molecule to ensure that the effects were observed only due to the imprinting features and not to the subsequent treatments undergone by the electrode. The MP template molecule was removed from the MIP film by CV scanning three times in PBS (pH 7.0) solution at room temperature. The complete removal of MP from the electropolymerized film was verified electrochemically. Fig. 3C shows the process of template removal by CV between 0.3 and -0.85 V with the scan rate of 100 mV s^{-1} in PB7 containing 0.1 M KCl. It indicated that the template molecule was easily to be removed from composite membrane. In contrast, for the Non-MIP-GCE (No shows), the redox current almost do not appears, because the FuAuNP-ATP-AuNP-MCNT film covered the surface of the GCE prepared in the absence of MP where no cavities with binding sites are obtained.

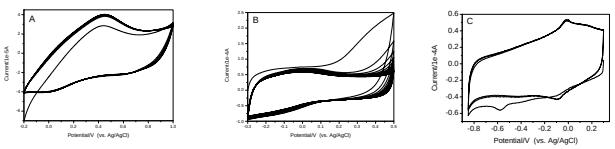

Fig. 3. (A) CV of AuNP electrodeposit onto MCNT/GCE in 0.2 M Na_2SO_4 solution containing 1 mM $HAuCl_4$ with a scan rate of 50 mV s^{-1} for 6 cycles. (B) CV corresponding to the electropolymerization of the FuAuNP on MP-ATP-AuNP-MCNT/GCE in the presence of 0.1 M PBS(pH=7.4) containing 1 mg mL^{-1} FuAuNP and 0.2 mg mL^{-1} MP with a scan rate of 50 mV s^{-1}. (C) The template was removed from the

imprinted polymer by CV in PB7 with a scan rate of 100 mV s^{-1}.

Electrochemical Measurements

Cyclic voltammetry (CV) and liner sweep voltammetry (LSV) measurements were performed in the potential range from 0.3 to -0.8V with a scan rate of 50mVs^{-1}. The electrochemical cell was connected to a VMP2 Multi-potentiostat with interfaced to a PC. An electrochemical impedance software EC-Lab was used to carry out impedance measurements. EIS was scanned at the formal potential of 0.25 V in the frequency range from 100 kHz to 100 mHz, using an AC voltage of 5mV amplitude. A simple equivalent circuit could be used to simulate the experimental EIS data gained from the modified GCE coated with a less conductive polymeric film. The impedance data (Rct) thus obtained were fitted to the R(Q(RW)) equivalent circuit using the ZsimpWin (Princeton Applied Research) program. All measurements were performed at room temperature.

Real samples preparation

Apple and cucumber samples were obtained from the supermarket (Lanzhou, China). The real samples were prepared as follows: peel the samples, and chop them into small pieces. Extraction of 10 g of the homogenized sample was performed with ethanol (30mL). The extract was simply filtered through a membrane filter and evaporated to dryness. And then ethanol (2 mL) was added. After mixing, the solution was diluted to 100 mL with 0.1 M PBS (pH=7.0) solution. Spiking of the sample was achieved by injecting MP stock solution into the sample and then homogenizing.

Results and discussion

Preparation of FuAuNP-ATP-MIP-AuNP-MCNT/GCE

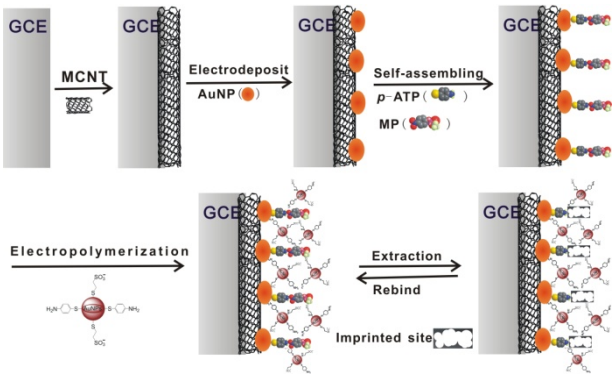

Scheme 2. Schematic representation of MP MIP sensor fabrication process.

Scheme 2 illustrates the preparation procedures of the FuAuNP-ATP-MIP- AuNP-MCNT/GCE. Prior to the polymerization, the AuNP-MCNT/GEC was immersed into *p*-ATP and MP solution for 2h. A self-assembled monolayer of *p*-ATP molecules was formed on the AuNP surface by Au-S bonds between gold and the thiol groups (-SH) of *p*-ATP molecules. The *p*-ATP monolayer was chemisorbed on the AuNP and exposed an array of amino groups towards the solution. Then, MP molecules in solution phase could be assembled onto the surface of *p*-ATP-AuNP-MCNT/GCE by hydrogen bond interactions between amino groups (–NH_2) of *p*–ATP and nitro(–NO_2) groups of MP. The intermolecular interactions among *p*-ATP, MP and FuAuNP could be confirmed by UV absorbance spectra. The maximum absorption wavelength of *p*-ATP showed red shifted in the presence of MP, and the maximum absorbance of *p*-ATP also increased with the addition of MP (See Fig. 4). They demonstrated that the formation of hydrogen bond interactions between the amino group (–NH_2) of *p*-ATP and nitro(–NO_2) groups of MP are formed in the system. Therefore, the strong hydrogen bond interactions would drive MP molecules to assemble onto the surface of the *p*-ATP modified electrode. And then, MP are embedded into the imprinted ATP-FuAuNP membranes on AuNP-MCNT/GCE to form surface imprinted sites, which would increase the amount of imprinted sites on the electrode surface and enhance sensitivity and selectivity of the sensor.

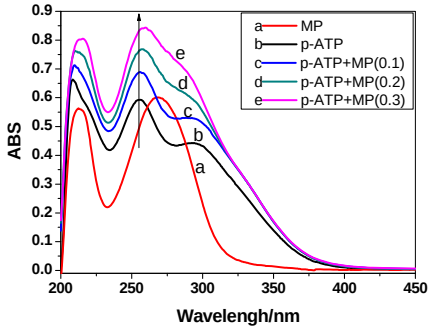

Fig. 4. UV spectra of MP(a), *p*-ATP(b), different amounts of MP into 0.067 mg mL^{-1} ATP solution(c,d,e).

Morphological characterization of the FuAuNP-ATP-MIP-AuNP- MCNT/GCE

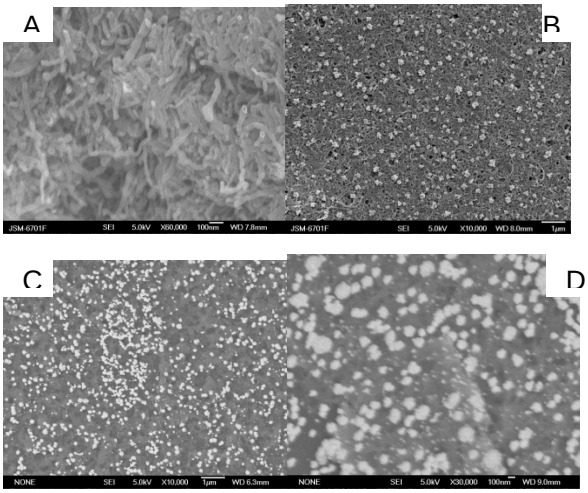

Fig. 5. SEM images of MCNT(A), AuNP-MCNT(B), and FuAuNP-ATP-MIP-AuNP-MCNT(C and D)

The surface morphologies of the different films modified are studied by means of SEM. Fig. 5 shows the SEM images of MCNT (Fig. 5A), AuNP-MCNT (Fig. 5B) and FuAuNP-ATP-MIP-AuNP-MCNT composites (Fig. 5C and D at different resolution). Homogeneous spaghetti-like tangled MCNT (Fig. 5A) decorated with a little of AuNP was observed in Fig. 5B. The diameter of the nanoparticles was between 20 and 50 nm. After self-assembling and electropolymerizing the FuAuNP, it was

found that the FuAuNP nanoparticles distributed uniformly between MCNT and AuNP, the diameter of the FuAuNP was less than 10 nm (Fig. 5C, D). The 3-dimensional structure was formed after AuNP decorated MCNT were further modified with MIP-ATP-FuAuNP on the electrode surface. The recognition sites, conductivity and specific surface area of the electrode are improved by the decoration nanocomposites effectively.

Electrochemical characterization of the FuAuNP-ATP-MIP-AuNP- MCNT/GCE

CV and EIS experiments are used to characterize the different modified electrodes in 5 mM $[Fe(CN)_6]^{3-}$/$[Fe(CN)_6]^{4-}$ containing 0.1 M KCl solution(see Fig. 6A). The reversible one-electron redox behavior of ferricyanide ions is observed on the bare GCE. After being modified with MCNT, the peak current of $[Fe(CN)_6]^{3-}$/$[Fe(CN)_6]^{4-}$ is increased. Also, becsuse of AuNP deposition on the MCNT/GCE, the peak current of $[Fe(CN)_6]^{3-}$/$[Fe(CN)_6]^{4-}$ increase again. Thus, the introduction of AuNP-MCNT hybrid play a role in the increasement of the electroactive surface area and provide a conducting bridge for the electron-transfer of $[Fe(CN)_6]^{3-}$/$[Fe(CN)_6]^{4-}$. The FuAuNP-ATP-MIP-AuNP-MCNT composite membrane is porous with fine conductivity and large specific surface area, so the peak current of $[Fe(CN)_6]^{3-}$/$[Fe(CN)_6]^{4-}$ increase again.

EIS is an effective method for studying interfacial properties of modified electrodes. Nyquist plots of GCE, MCNT/GCE, AuNP-MCNT/GCE, and FuAuNP-ATP-MIP-AuNP-MCNT/GCE are shown in Fig. 5B. The impedance data (R_{ct}) are obtained by fitted to the R(Q(R(Q(RW)))) equivalent circuit model (inset of Fig. 6B) using the ZsimpWin program. The impedance data obtained contain the electron transfer process (modeled as a resistance to charge transfer, R_{ct}) and the diffusion process (modeled as the Warburg-type impedance, W). Both R_{ct} and W are in parallel with the constant phase angle element (Q)[70]. The angle of the line in semi-infinite region is observed less than 45°. This is a typical porous electrode surface character. The above EIS results reveal that AuNP-MCNT/GCE exhibits a improved charge transfer rate than that of bare GCE. The EIS of FuAuNP-ATP-MIP-AuNP-MCNT/GCE behaves like a porous electrode[67], which are consistent with that of CV.

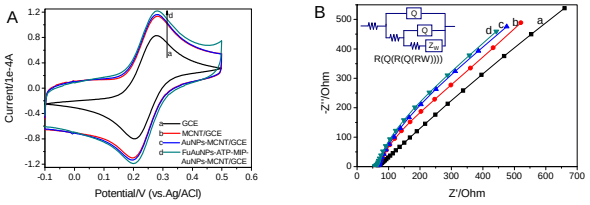

Fig. 6. (A) CVs of GCE(a), MCNT/GCE(b), AuNP-MCNT/GCE(c), and FuAuNP- ATP-MIP-AuNP-MCNT/GCE(d) in 5 mM $[Fe(CN)_6]^{3-}$/$[Fe(CN)_6]^{4-}$ containing 0.1 M KCl solution with a scan rate of 50 mV s^{-1}. (B) Nyquist plots of GCE(a), MCNT/GCE(b), AuNP-MCNT/GCE(c), and FuAuNP-ATP-MIP-AuNP-MCNT/ GCE(d) in 5 mM $[Fe(CN)_6]^{3-}$/$[Fe(CN)_6]^{4-}$ containing 0.1 M KCl solution. The frequency range is from 100 mHz to 100 kHz. Inset of B is equivalent circuit model.

Effect of solution pH on the peak currents and peak potential

The effects of solution pH on peak currents and peak potentials were performed by linear stripping sweep voltammetry (LSSV) and the results were shown in Fig. 7. With the increase of pH value, the peak potentials shift negatively (shown in Fig. 7b). At the same time, the experimental results also show that pH has a significant influence on the cathodal peak current of MP on MIP-AuNP-MCNT-GCE (shown in Fig. 7a). It can be seen that the values of the peak current changes with the different pH in the range from 3.5 to 11. Obviously, the maximum response of peak current appears at pH 7.0. In this work, the optimum pH value of 7.0 was selected in the following experiments.

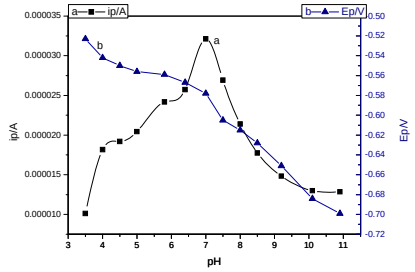

Fig. 7. LSSV response of the MIP sensor in 1 μg/mL MP containing PBS at various pHs: 3.5, 4.0, 4.5, 5.0, 5.8, 6.4, 7.0, 7.5, 8.0, 8.5, 9.2, 10.1, 10.9.

Effects of scan rate and accumulation time on the electrochemical response of MP

The CV curves of MP on the FuAuNP-ATP-MIP-AuNP-MCNT/GCE were investigated at different scan rates (see Fig. 8). The reduction peak currents for 5 ng mL^{-1} MP in 0.1 M PBS (pH 6.8) are linearly proportional to the scan rates from 50 to 450 mV s^{-1} with a linear regression equation of $i_p = 3.781 \times 10^{-6} + v$ 7.72502×10^{-8} (r=0.9993), it is indicated that the electron transfer processes are controlled by surface adsorption process. In addition, the reduction peak potentials shift with the increase of scan rate, which can be attributed to the catalytic effects of surface of imprinted composite on template molecules. The proposed catalysis mechanism is shown in the following equation (1)-(3)[71-73].

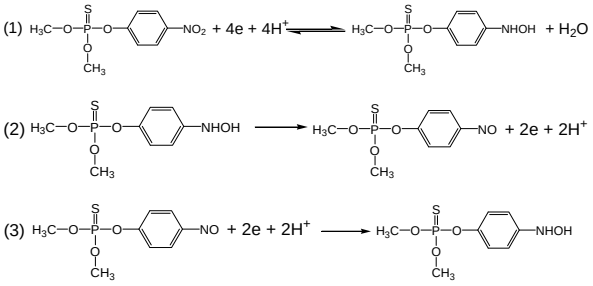

Scheme 3. The electrochemical reaction mechanism of MP.

It is reported previously that different incubation time may cause different responses. Hence the effect of incubation time on peak current was investigated by kinetic experiment in this work. The incubation step is usually a simple and effective way to enhance the sensitivity of the imprinted sensor. Fig. 9 shows the change of LSSV with different incubation time. The figure shows that the LSSV peak currents increase with the increase of incubation time. When the incubation time less than 4 min, the peak current increase rapidly, however, it increase slowly after 4 min. Considering the efficiency and reproducibility of experiment, the incubation time of 6 min is selected in subsequent experiment.

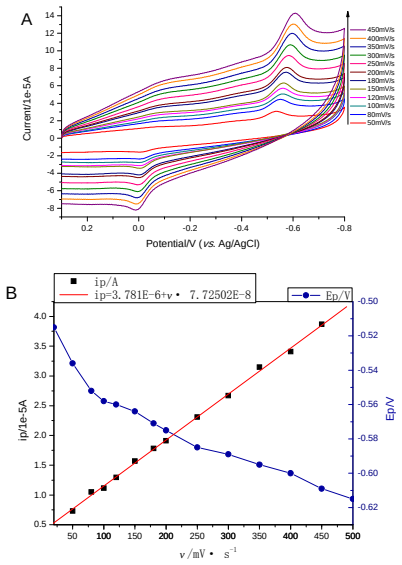

Fig. 8. Effect of scan rate(v) to CV on the FuAuNP-ATP-MIP-AuNP-MCNT/GCE in 0.1 M PBS containing 5 ng mL^{-1} MP (pH 7.0). (A) CVs with different scan rate(v). (B) The peak currents(ip) and peak potentials(Ep) *vs.* scan rate(v).

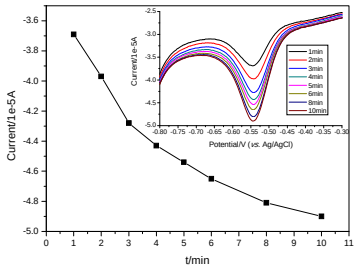

Fig. 9. LSSV response with different times of preconcentration.

Electrochemical detection of MP

In this study, LSSV was employed to evaluate the performance of sensor on detection of MP. After FuAuNP-ATP-MIP-AuNP-MCNT/GCE is immersed in different concentrations of MP solutions for 6 min, a significant peak current increase is then observed in Fig. 10. It is seen there were two linear relationships between current and MP concentration from 0.1 to 1.1 ng mL^{-1} (R = 0.9983) and 1.1 to 11 ng mL^{-1} (R = 0.9996). Therefore, two different slopes of linear curves are obtained, resulting from the different mechanism of molecular recognition in two different ranges of concentration. In the range of 0.1 to 1.1 ng mL^{-1}, because of the low concentration levels of MP in solution, hydrogen bonding adsorption is the main mode of the action between the MP molecular and binding sites. As a result, the large slope of the linear relationship is obtained. However, when the concentration of MP is high in the solution, strong Vander Waals force between MP molecular occurs besides hydrogen bonding adsorption. It has deleterious effects for template molecules to reach the imprinted sites, leading to a low slop in the range of high concentration. Most importantly, it is noteworthy that the detection limit of 0.08 ng mL^{-1} can be achieved, which is the lowest value reported so far, indicating high sensitivity of the sensor designed in this paper for the detection of MP[31].

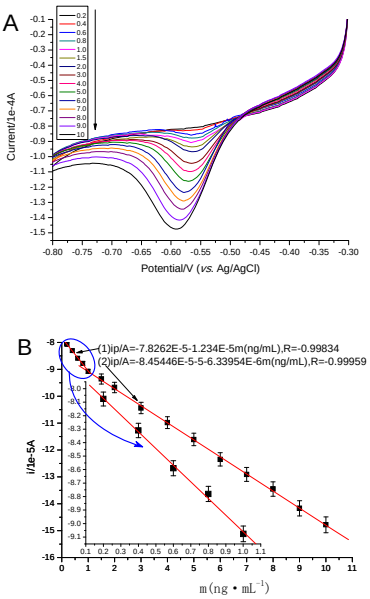

Fig. 10. (A) LSSV responses of FuAuNP-ATP-MIP-AuNP-MCNT/GCE to different concentration of MP in 0.1M PBS with a scan rate 50 mV s^{-1}. (B) Calibration curves corresponding to analysis of MP.

Selectivity of the MIP enzymeless sensor

The anti-interference ability of the proposed sensor has also been studied. In order to detect the selectivity of the MIP sensor, four types of organophosphate pesticides (phoxim, malathoate, omethoate and (2,4-dichlorophenoxy) acetic acid (2,4-D)) which have a similar structure to MP are selected to conduct the control experiments.

The experimental results show that the FuAuNP-ATP-MIP-AuNP-MCNT/GCE in 0.1 M PBS containing 5 ng mL^{-1} MP (pH 7.0) gains no obvious interferences from organophosphate pesticides such as phoxim, malathoate, omethoate and 2,4-D， and other inorganic ions (PO_4^{3-}, SO_4^{2-}, NO_3^-). These results clearly indicate that the MIPs sensor have a good recognition ability towards the target molecule. The high specificity is mainly attributed to the unique binding modes of the imprinted sites to the target molecule, eliminating the possibility to bind with other analogues.

Reproducibility and Stability of the Molecularly Imprinted Sensor

To characterize the reproducibility of the sensor, a series of repetitive measurements were carried out in 0.1M PBS containing 5 ng mL^{-1} MP (pH 7.0) under identical experimental conditions. The electrode can be renewed easily by CV in PBS after each determination. For 5 ng mL^{-1} MP, relative peak current change is obtained by the use of each sensors. Relative standard deviation (RSD) of 4.2% (n=5) is obtained and indicated good reproducibility. The stability of the sensors is an important factor for practical applications. It is found no obvious change in peak current is observed after the MIP sensor is stored at 4 ℃ over 10 days. After one month, it decreased by approximately 43%. This result indicates that the MIP sensor possesses excellent stability.

Sample analysis

The feasibility of the MIP sensor for practical applications was investigated by the determination of MP in distilled water, tap water, apple and cucumber samples according to the proposed method. None of these real samples had electrochemistry responses when analyzed by using the MIP sensor. They were spiked with different levels of MP and the results are presented in Table 1.

Table 1 The determination results of MP in real samples (n=5)

Sample	Spiked /ng/mL	Found / ng/mL	Recovery (%)	RSD(%)
Distilled water				
1	0.50	0.493	98.6	1.8
2	1.00	1.012	101.2	2.0
Tap water				
1	0.50	4.856	97.12	2.3
2	1.00	1.046	104.6	2.6
Apple				
1	0.50	0.476	95.2	3.2
2	1.00	1.054	105.4	3.5
3	5.00	5.286	105.7	3.7
Cucumber				
1	0.50	0.483	96.6	2.8
2	1.00	1.052	105.2	3.3
3	5.00	4.795	95.9	3.8

As shown in Table 1, the sensor used to detect MP is not greatly affected by MP in different samples. The average recoveries ranges between 95.2% and 105.7%, with less than 3.8% RSD (n=5). The presented results demonstrate that the proposed method is a promising approach for MP determination in real samples.

As shown in Table 2, the proposed sensor was compared with other published methods. It can be seen that the sensor exhibits remarkable advantages, such as higher sensitivity, wider linear range and lower detection limit, which provide an attractive perspective for its wide application.

Conclusions

A novel electrochemical sensing strategy for sensitive detecting MP was developed. The proposed method relies on the hydrogen bond interactions among MP, *p*-ATP and FuAuNP. The tailor-made cavities formed in the imprinted film showed good selectivity toward MP. The reproducibility, repeatability and stability of the MIP sensor were satisfactory. The good sensitivity and selectivity on the sensor is attributed to following reasons. Firstly, the employment of MCNT in the Nafion film enlarges the electro-active surface area. Secondly, the nano-hybrid materials of AuNP-MCNT improve the conductivity of the assembled film and increase the quantity of template molecule in the unit area. Finally, the 3-dimensional structure is formed by electro-polymerization and self-assembly of FuAuNP-ATP-MIP-AuNP-MCNT on the electrode surface. The network-like nanocomposite not only provided a microenvironment to increase the recognition sites, conductivity and specific surface area of electrode, but also exhibited a strong synergetic effect on improving the sensing properties of MP. Therefore, this novel, fast and facile strategy reported herein can be further expected to fabricate various electrochemical sensors for detecting pesticide residuals and other environmentally deleterious chemicals.

Table 2. Comparison with other methods for the determination of MP

Methods	Linear range	LOD/M	Ref.
MWCNTs MIP/GCE	2.0×10^{-7}–1.0×10^{-5} M	6.7×10^{-8} M	39
MWCNTs–PAAM/GCE	5.0×10^{-9}–1.0×10^{-5} M	2.0×10^{-9} M	74
Surfactant–clay/GCE	4.0×10^{-7}–8.5×10^{-6} M	7.0×10^{-8} M	75
ZrO_2/CPE	1.9×10^{-8}–1.1×10^{-5} M	7.6×10^{-9} M	76
Pd/MWCNTs/GCE	3.8×10^{-7}–5.3×10^{-5} M	1.9×10^{-7} M	77
Au–nafion/GCE	5.0×10^{-7}–1.2×10^{-4} M	1.0×10^{-7} M	78
pSC_6–AgNPs/GCE	1.0×10^{-8}–8.0×10^{-5} M	4.0×10^{-9} M	79
OMC/GCE	9.0×10^{-8}–6.1×10^{-5} M	7.6×10^{-9} M	80
Silicate–CTAB/GCE	1.0×10^{-7}–1.0×10^{-4} M	1.0×10^{-8} M	81
C/p–NiTSPc/CFME	3.8×10^{-8}–3.8×10^{-5} M	1.5×10^{-7} M	82
MWCNTs–chitosan/GCE	1.9×10^{-7}–7.6×10^{-6} M	1.9×10^{-8} M	83
Au/MWCNTs electrode	1.9×10^{-6}–6.1×10^{-5} M	1.9×10^{-7} M	84
Imprinted PQu–PRe–AuNPs/GCE	7×10^{-8}–1×10^{-6} M	3.4×10^{-10} M	85
GR–CS/GCE	4.0 ng mL^{-1}–400 ng mL^{-1}	0.8 ng mL^{-1}	86
AChE–SiSG–CPE	0.1–1 ppb	0.04 ppb	87
AChE–AuNPs–PPy/GCE	0.019×10^{-6}–0.45×10^{-6}M	7.6×10^{-7}M	88
Optical microbial biosensor	$4–80\times10^{-6}$M	3×10^{-7}M	16
MPH–Sp@AuNPs/MWNTs/GCE	0.001–5× 10^{-6}g/mL	0.3 ng/mL	89
Matrix solid phase dispersion	–	4×10^{-9} M	90
β–CD–graphene/GCE	0.3–1.0 ppb, 1.0–500 ppb	0.05 ppb	12
HNC–CNP–CPE	1.55×10^{-9}–3.67×10^{-6}	4.70×10^{-10}	91
LDHs–GNs/GCE	0.003–0.05 and 0.1–1.0μg mL^{-1}	0.6 ng mL^{-1}	92
nano–Au/SDBS/GCE	5.0×10^{-7}–1.0×10^{-4} M	8.6×10^{-8} M	93
FuAuNP–ATP–MIP–AuNP–MCNT/GCE	0.1-1.1 and 1.1-11 ng mL^{-1}	0.08 ng mL^{-1}	This work

Acknowledgements

This work was supported by the National Natural Science Foundation of China (No. 21175108, 20965007, 21265018), the Applied Chemistry Key Subject of Gansu Province (No. GSACKS20130113), the Science and Technology Support Projects of Gansu Province (No.1011GKCA025), the Natural Science Foundation of Gansu Province (No. 1208RJZM289) , the Science and Technology Projects of Qingyang (No. KH201302) and the Doctor Foundation of Longdong University(No. XYBY07).

References

1. J. Sherma, *Anal. Chem.*, 1987, **59**, 18R-31R.

2. G. Gervais, S. Brosillon, A. Laplanche and C. Helen, *J. Chromatogr. A*, 2008, **1202**, 163-172.
3. D. Du, J. Wang, J. N. Smith, C. Timchalk and Y. Lin, *Anal. Chem.*, 2009, **81**, 9314-9320.
4. G. Liu and Y. Lin, *Anal. Chem.*, 2006, **78**, 835-843.
5. E. Borrás, P. Sánchez, A. Muñoz and L. A. Tortajada-Genaro, *Anal. Chim. Acta*, 2011, **699**, 57-65.
6. M. R. Khalili-Zanjani, Y. Yamini, N. Yazdanfar and S. Shariati, *Anal. Chim. Acta*, 2008, **606**, 202-208.
7. A. Garrido Frenich, J. L. Martínez Vidal, A. D. Cruz Sicilia, M. J. González Rodríguez and P. Plaza Bolaños, *Anal. Chim. Acta*, 2006, **558**, 42-52.
8. M. J. Hengel and M. Miller, *J. Agric. Food Chem.*, 2008, **56**, 6851-6856.
9. O. Leoni, R. Iori and S. Palmieri, *J. Agric. Food Chem.*, 1991, **39**, 2322-2326.
10. H. Guan, W. E. Brewer and S. L. Morgan, *J. Agric. Food Chem.*, 2009, **57**, 10531-10538.
11. J. W. Wong, M. G. Webster, C. A. Halverson, M. J. Hengel, K. K. Ngim and S. E. Ebeler, *J. Agric. Food Chem.*, 2003, **51**, 1148-1161.
12. S. Wu, X. Lan, L. Cui, L. Zhang, S. Tao, H. Wang, M. Han, Z. Liu and C. Meng, *Anal. Chim. Acta*, 2011, **699**, 170-176.
13. A. Crew, D. Lonsdale, N. Byrd, R. Pittson and J. P. Hart, *Biosens. Bioelectron.*, 2011, **26**, 2847-2851.
14. J. Kumar and S. F. D'Souza, *Biosens. Bioelectron.*, 2010, **26**, 1292-1296.
15. L. B. O. dos Santos and J. C. Masini, *Anal. Chim. Acta*, 2008, **606**, 209-216.
16. J. Kumar, S. K. Jha and S. F. D'Souza, *Biosens. Bioelectron.*, 2006, **21**, 2100-2105.
17. C. Wang, X. Li, Y. Liu, Y. Guo, R. Xie, W. Gui and G. Zhu, *J. Agric. Food Chem.*, 2010, **58**, 5658-5663.
18. M. Mascini, M. Sergi, D. Monti, M. D. Carlo and D. Compagnone, *Anal. Chem.*, 2008, **80**, 9150-9156.
19. S. Guo, J. Li, W. Ren, D. Wen, S. Dong and E. Wang, *Chem. Mater.*, 2009, **21**, 2247-2257.
20. S. Xu, C. Guo, Y. Li, Z. Yu, C. Wei and Y. Tang, *J. Hazard. Mater.*, 2014, **264**, 34-41.
21. L. Zhao, F. Zhao and B. Zeng, *Sens. Actuators, B*, 2013, **176**, 818-824.
22. G. Mustafa and P. A. Lieberzeit, *RSC Advances*, 2014, **4**, 12723-12728.
23. M. Andac and A. Denizli, *RSC Advances*, 2014, **4**, 31130-31141.
24. P. J. R. Roche, S. M. Ng, R. Narayanaswamy, N. Goddard and K. M. Page, *Sens. Actuators, B*, 2009, **139**, 22-29.
25. K. Haupt and K. Mosbach, *Chem. Rev.*, 2000, **100**, 2495-2504.
26. M. T. Muldoon and L. H. Stanker, *Anal. Chem.*, 1997, **69**, 803-808.
27. L. Ye and K. Mosbach, *Chem. Mater.*, 2008, **20**, 859-868.
28. Z.-p. Yang and C.-j. Zhang, *Sens. Actuators, B*, 2009, **142**, 210-215.
29. B. Wu, Z. Wang, Z. Xue, X. Zhou, J. Du, X. Liu and X. Lu, *Analyst*, 2012, **137**, 3644-3652.
30. B. Wu, Z. Wang, D. Zhao and X. Lu, *Talanta*, 2012, **101**, 374-381.
31. H. Li, Z. Wang, B. Wu, X. Liu, Z. Xue and X. Lu, *Electrochim. Acta*, 2012, **62**, 319-326.
32. W. Zhihua, L. Xiaole, Y. Jianming, Q. Yaxin and L. Xiaoquan, *Electrochim. Acta*, 2011, **58**, 750-756.
33. C. Algieri, E. Drioli, L. Guzzo and L. Donato, *Sensors-basel*, 2014, **14**, 13863-13912.
34. J. Dai, X. Wei, Z. Cao, Z. Zhou, P. Yu, J. Pan, T. Zou, C. Li and Y. Yan, *RSC Advances*, 2014, **4**, 7967-7978.
35. F. Duan, C. Chen, G. Wang, Y. Yang, X. Liu and Y. Qin, *RSC Advances*, 2014, **4**, 1469-1475.
36. M. Riskin, R. Tel-Vered, T. Bourenko, E. Granot and I. Willner, *J. Am. Chem. Soc.*, 2008, **130**, 9726-9733.
37. B. M. Jung, M. S. Kim, W. J. Kim and J. Y. Chang, *Chem. Commun.*, 2010, **46**, 3699-3701.
38. Y. Liang, L. Gu, X. Liu, Q. Yang, H. Kajiura, Y. Li, T. Zhou and G. Shi, *Chem.-Eur. J.*, 2011, **17**, 5989-5997.
39. D. Zhang, D. Yu, W. Zhao, Q. Yang, H. Kajiura, Y. Li, T. Zhou and G. Shi, *Analyst*, 2012, **137**, 2629-2636.
40. S. Iijima, *Nature*, 1991, **354**, 56-58.
41. B. J. Privett, J. H. Shin and M. H. Schoenfisch, *Anal. Chem.*, 2010, **82**, 4723-4741.
42. C. B. Jacobs, M. J. Peairs and B. J. Venton, *Anal. Chim. Acta*, 2010, **662**, 105-127.
43. F. C. Moraes, I. Cesarino, V. Cesarino, L. H. Mascaro and S. A. S. Machado, *Electrochim. Acta*, 2012, **85**, 560-565.
44. B. B. Prasad and I. Pandey, *Electrochim. Acta*, 2013, **88**, 24-34.
45. R. N. Goyal, V. K. Gupta, M. Oyama and N. Bachheti, *Electrochem. Commun.*, 2005, **7**, 803-807.
46. A. N. Shipway, E. Katz and I. Willner, *Chemphyschem*, 2000, **1**, 18-52.
47. Y. Guo, S. Guo, Y. Fang and S. Dong, *Electrochim. Acta*, 2010, **55**, 3927-3931.
48. S. Guo and S. Dong, *TrAC, Trends Anal. Chem.*, 2009, **28**, 96-109.
49. Y. Lin, K. A. Watson, S. Ghose, J. G. Smith, T. V. Williams, R. E. Crooks, W. Cao and J. W. Connell, *The Journal of Physical Chemistry C*, 2009, **113**, 14858-14862.
50. Y. Lin, K. A. Watson, M. J. Fallbach, S. Ghose, J. G. Smith, D. M. Delozier, W. Cao, R. E. Crooks and J. W. Connell, *ACS Nano*, 2009, **3**, 871-884.
51. K. A. Mahmoud, S. Hrapovic and J. H. T. Luong, *ACS Nano*, 2008, **2**, 1051-1057.
52. F. Valentini, A. Amine, S. Orlanducci, M. L. Terranova and G. Palleschi, *Anal. Chem.*, 2003, **75**, 5413-5421.
53. A. V. Ellis, K. Vijayamohanan, R. Goswami, N. Chakrapani, L. S. Ramanathan, P. M. Ajayan and G. Ramanath, *Nano Lett.*, 2003, **3**, 279-282.
54. T. Alizadeh, M. Zare, M. R. Ganjali, P. Norouzi and B. Tavana, *Biosens. Bioelectron.*, 2010, **25**, 1166-1172.
55. J. Li, F. Jiang, Y. Li and Z. Chen, *Biosens. Bioelectron.*, 2011, **26**, 2097-2101.
56. F. T. C. Moreira, A. H. Kamel, J. R. L. Guerreiro and M. G. F. Sales, *Biosens. Bioelectron.*, 2010, **26**, 566-574.
57. F. L. Dickert, M. Tortschanoff, W. E. Bulst and G. Fischerauer, *Anal. Chem.*, 1999, **71**, 4559-4563.
58. E. Pardieu, H. Cheap, C. Vedrine, M. Lazerges, Y. Lattach, F. Garnier, S. Remita and C. Pernelle, *Anal. Chim. Acta*, 2009, **649**, 236-245.
59. A. L. Rogach, A. Kornowski, M. Gao, A. Eychmüller and H. Weller, *J. Phys. Chem. B*, 1999, **103**, 3065-3069.
60. J. Luo, M. M. Maye, V. Petkov, N. N. Kariuki, L. Wang, P. Njoki, D. Mott, Y. Lin and C.-J. Zhong, *Chem. Mater.*, 2005, **17**, 3086-3091.
61. D. Balogh, R. Tel-Vered, R. Freeman and I. Willner, *J. Am. Chem. Soc.*, 2011, **133**, 6533-6536.
62. M. Frasconi, R. Tel-Vered, M. Riskin and I. Willner, *J. Am. Chem. Soc.*, 2010, **132**, 9373-9382.
63. M. Riskin, R. Tel-Vered, O. Lioubashevski and I. Willner, *J. Am. Chem. Soc.*, 2009, **131**, 7368-7378.
64. I. Willner, B. Willner and R. Tel-Vered, *Electroanal.*, 2011, **23**, 13-28.
65. J. Zhang, M. Riskin, R. Freeman, R. Tel-Vered, D. Balogh, H. Tian and I. Willner, *ACS Nano*, 2011, **5**, 5936-5944.
66. M. Shen, S. H. Wang, X. Shi, X. Chen, Q. Huang, E. J. Petersen, R. A. Pinto, J. R. Baker and W. J. Weber, *The Journal of Physical Chemistry C*, 2009, **113**, 3150-3156.
67. B. Wu, Z. Wang, z. Xue, X. Zhou, J. Du, X. Liu and X. Lu, *Analyst*, 2012, **137**, 3644-3652.
68. I. Rubinstein, J. Rishpon, E. Sabatani, A. Redondo and S. Gottesfeld, *J. Am. Chem. Soc.*, 1990, **112**, 6135-6136.
69. Z. Huang, F. Chen, P. A. Bennett and N. Tao, *J. Am. Chem. Soc.*, 2007, **129**, 13225-13231.
70. C.-N. Cao and J.-Q. Zhang, *An Introduction to Electrochemical Impedance Spectroscopy*, Sciences Press, Beijing, 2002.
71. X. Tan, B. Li, K. Liew and C. Li, *Biosens. Bioelectron.*, 2010, **26**, 868-871.
72. D. Du, X. Ye, J. Zhang, Y. Zeng, H. Tu, A. Zhang and D. Liu, *Electrochem. Commun.*, 2008, **10**, 686-690.
73. G. Liu and Y. Lin, *Anal. Chem.*, 2005, **77**, 5894-5901.
74. Y. Zeng, D. Yu, Y. Yu, T. Zhou and G. Shi, *J. Hazard. Mater.*, 2012, **217-218**, 315-322.

75. H. L. Tcheumi, I. K. Tonle, E. Ngameni and A. Walcarius, *Talanta*, 2010, **81**, 972-979.
76. H. Parham and N. Rahbar, *J. Hazard. Mater.*, 2010, **177**, 1077-1084.
77. B. Huang, W.-D. Zhang, C.-H. Chen and Y.-X. Yu, *Microchim Acta*, 2010, **171**, 57-62.
78. T.-F. Kang, F. Wang, L.-P. Lu, Y. Zhang and T.-S. Liu, *Sens. Actuators, B*, 2010, **145**, 104-109.
79. Y. Bian, C. Li and H. Li, *Talanta*, 2010, **81**, 1028-1033.
80. D. Pan, S. Ma, X. Bo and L. Guo, *Microchim Acta*, 2011, **173**, 215-221.
81. S. Xia, J. Zhang and C. Li, *Anal. Bioanal. Chem.*, 2010, **396**, 697-705.
82. I. Tapsoba, S. Bourhis, T. Feng and M. Pontié, *Electroanal.*, 2009, **21**, 1167-1176.
83. D. Du, M. Wang, J. Zhang, J. Cai, H. Tu and A. Zhang, *Electrochem. Commun.*, 2008, **10**, 85-89.
84. J.-C. Ma and W.-D. Zhang, *Microchim Acta*, 2011, **175**, 309-314.
85. H. Li, Z. Wang, B. Wu, X. Liu, Z. Xue and X. Lu, *Electrochim. Acta*, 2012, **62**, 319-326.
86. S. Yang, S. Luo, C. Liu and W. Wei, *Colloids Surf. B. Biointerfaces*, 2012, **96**, 75-79.
87. P. Raghu, T. Madhusudana Reddy, B. E. Kumara Swamy, B. N. Chandrashekar, K. Reddaiah and M. Sreedhar, *J. Electroanal. Chem.*, 2012, **665**, 76-82.
88. J. Gong, L. Wang and L. Zhang, *Biosens. Bioelectron.*, 2009, **24**, 2285-2288.
89. S. Chen, J. Huang, D. Du, J. Li, H. Tu, D. Liu and A. Zhang, *Biosens. Bioelectron.*, 2011, **26**, 4320-4325.
90. B. Albero, C. Sánchez-Brunete and J. L. Tadeo, *J. Agric. Food Chem.*, 2003, **51**, 6915-6921.
91. B. J. Sanghavi, G. Hirsch, S. P. Karna and A. K. Srivastava, *Anal. Chim. Acta*, 2012, **735**, 37-45.
92. H. Liang, X. Miao and J. Gong, *Electrochem. Commun.*, 2012, **20**, 149-152.
93. C. Li, Z. Wang and G. Zhan, *Colloids Surf. B. Biointerfaces*, 2011, **82**, 40-45.

TOC

A molecularly imprinted electrochemical enzymeless sensor based on functionalized gold nanoparticles decorated carbon nanotubes for methyl-parathion detection

Bowan Wu[a,b], Lijie Hou[a], Miao Du[a], Tiantian Zhanga, Zhihua Wang[b], Zhonghua Xue[b], Xiaoquan Lu[b]*

Abstract

Functionalized gold nanoparticles (FuAuNP) have a bright future because of its specific functional groups. *p*-Aminothiophenol (*p*-ATP) possesses double functional groups which can be used to form S-Au bond and oligoaniline. Based on molecular imprinting technology and electrochemical technology, a novel enzymeless Methy-parathion (MP) sensor is constructed with nanocomposites. The template molecule (MP) is embedded in imprinting sites by *p*-ATP molecular self-assembly and FuAuNP electro-polymerization. The imprinting effective sites and the conductive performance are improved by gold nanoparticles decorated carbon nanotubes nanocomposites (AuNP-MCNT). The linear relationships between peak current and MP concentration are obtained in the range from 0.1 to 1.1 ng mL^{-1} and 1.1 to 11 ng mL^{-1} (respectively). The detection limit can be achieved as low as 0.08 ng mL^{-1} (3σ) with relative standard deviation 3.8% (n = 5). This sensor was also applied in the detection of MP in appler and vegetables with average recoveries between 95.2% and 105.7% (RSD < 5%). The results mentioned above show that the novel electrochemical sensor is an ideal device for the real-time determination of MP in real samples.

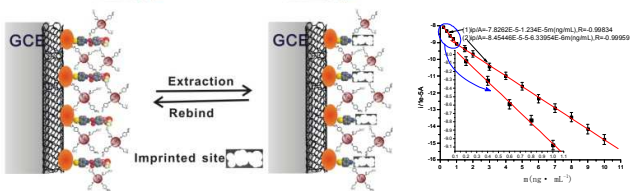

Schematic MP MIP sensor and the possible mechanism.